Kinematic Analysis of Non-steering Four-wheel Vehicles

Giorgio Figliolini, Chiara Lanni and Luciano Tomassi

Abstract This paper deals with the kinematic analysis of non-steering four-wheel vehicles and particular attention is devoted to the turning task around the central vertical axis. The four-wheel drives, one for each wheel, operate together to generate the chassis angular velocity because of the friction forces effect at the wheel-ground contact, which give a resulting moment around the central axis. In this operating context and also referring to wheeled mobile robots (WMRs), a three-dimensional quarter-vehicle kinematic model is proposed in the form of a spatial mechanism, which is composed by the supporting plane (ground) and the chassis-link, along with the corresponding front-right rigid wheel, chosen as reference. Therefore, a spatial kinematic analysis of a quarter-vehicle model, as derived by non-steering four-wheel vehicles, is proposed with the aim to investigate the best theoretical shape of each wheel, along with its rolling and sliding motions. Finally, first results on the full vehicle are also shown.

1 Introduction

There is a wide number of technical solutions for locomotion, such as multi-legged walking robots, which are biologically inspired since tending to imitate legged animals, as reported in [1], but also tracked and wheeled mobile robots (WMRs), which can move on flat and/or irregular terrains. The fundamentals regarding these general topics on robotic mechanical systems are theoretically treated in [2].

Giorgio Figliolini, Chiara Lanni and Luciano Tomassi.
DICEM, University of Cassino & Southern Lazio. e-mail: figliolini@unicas.it, lanni@unicas.it, luciano.tomassi@unicas.it

However, the WMRs have gained great interest in the last decades, because of their important applications in the field of robotics, including but not limited to autonomous navigation, warehouse automation and planetary exploration. In fact, they are more efficient in terms of energy consumption, require fewer and simpler mechanical components and consequently, WMRs are easier to build than legged or tracked robots, including actuation and control, which are also less complex. Of course, the most common wheeled vehicle is represented by the car that is a four-wheeled road vehicle, powered by a unique internal combustion engine and/or several electric drives. Nevertheless, as reported in [3], the car movements are very limited by the steering system, just think to the difficulties of the parking maneuvers, but this layout remains the safest solution in the application field of automotive. Moreover, the roll motion kinematic behavior of vehicles with double-wishbone and McPherson suspension systems, was analyzed in [4] and [5], respectively. Conversely, the wheeled mobile robotic field, which can find applications in the industrial environment, as for solving logistic problems in narrow spaces, but also in space exploration, agricultural machinery, military, including surveillance, reconnaissance, transportation, and even mine detection, as a safer alternative in hazardous environments, do not require specifically steering wheels, because WMRs move at much lower speed with respect to transportation vehicles. Thus, removing this important design specification, the attention of this paper is focused on non-steering four-wheel vehicles, such as WMRs, which are provided of four independent electric drives, one for each wheel, and thus, allowing the vehicle motion through a suitable wheel torque distribution, without the need of a mechanical steering device. In this general context, non-steering vehicles with particular wheel shapes, starting by the conventional cylindrical one, with tires or not, up to the omnidirectional (Mecanum) and/or ball wheels, are considered as further development of the proposed kinematic analysis. An interesting and recent state of art overview on different omnidirectional locomotion strategies is reported in [6], including the Mecanum wheels.

More in depth, some kinematic models of WMRs are formulated and analyzed in [7], while particular attention on WMRs with omnidirectional (Mecanum) wheels, is paid in [8, 9] dealing with several integrated aspects. Furthermore, Sreenivasan and Nanua [10] used a kinematic-geometric approach to study the first-order motion characteristics on even and uneven terrains, while Gracia and Tornero [11] considered four common types of wheels: fixed, orientable, castor, and Swedish. An overview on wheeled robots can be found on the Ch.17 of the book of Campion and Chung [12].

In this paper, a three-dimensional quarter-vehicle kinematic model with particular reference to WMRs, is proposed in the form of a spatial mechanism, which is composed by the supporting plane (ground) and the chassis-link, along with the corresponding front-right rigid wheel, that is chosen as reference. This approach is based on the application of the screw theory, likewise to what did previously for skew gears in [13, 14]. Thus, a spatial kinematic analysis of a quarter-vehicle model of non-steering four-wheel vehicles is proposed to investigate the best theoretical shape of each wheel and to analyze both rolling and sliding motions. First results on the full vehicle are also shown.

2 Non-steering four-wheel vehicle

Referring to Fig. 1, the orthogonal projections of non-steering four-wheel vehicle kinematic sketch is represented by including the main velocity vectors and diagrams.

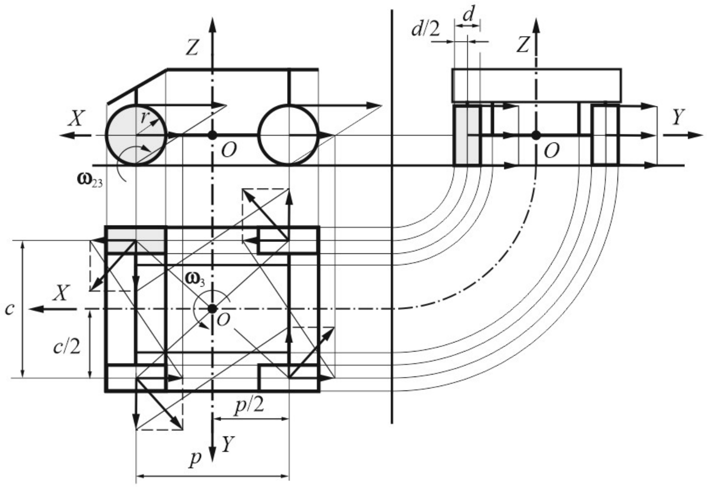

Fig. 1. Non-steering four-wheel vehicle kinematic sketch, velocity vectors included

In particular, the Cartesian reference frame *OXYZ* is assumed as attached to the vehicle chassis, which has the *X*-axis oriented along the proper longitudinal axis and toward the front side, the *Y*-axis belonging to the chassis plane and oriented toward the external lateral right-side, while the *Z*-axis is oriented upward to obtain a right-handed reference system. The main geometric characteristics of this non-steering vehicle are the pitch p and track c, along with the wheel radius r and thickness d.

Consequently, the four-wheel centers are located on the corresponding vertices of this rectangle with p and c edges, while the chassis center O is supposed to be located on its geometrical center, at height r by the ground, as shown on the front and lateral views of Fig. 1. Thus, a counter-clockwise turning maneuver around the vehicle central Z-axis, can be generated by operating the four electric drives, one for each wheel, properly, because of their non-steering characteristics. In particular, the vehicle chassis turns counter-clockwise around the Z-axis that takes the role of the Instant Screw Axis (ISA) of the whole non-steering vehicle. In other words, the right wheels pair rotates together with the same angular velocity vector $\boldsymbol{\omega}_{23}$ that is oriented toward the positive Y-axis, while the left wheels pair rotates together in opposite sense and thus, with $\boldsymbol{\omega}_{23}$ oriented along the negative Y-axis. This operation of the four-wheel drives generates the absolute angular velocity ω_3 of the vehicle, because of the friction forces effect at the wheel-ground contact, which give a resulting moment around the central Z-axis. However, a sliding contact of each non-steering wheel cannot be avoided, as sketched in Fig. 1 by referring to the velocity vectors and diagrams. In fact, observing the top view of the sketch that illustrates the rectangular footprint of the chassis and the placement of the four wheels, the angular velocity vector $\boldsymbol{\omega}_3$ is given by the velocity vector field that is generated by the four wheel-ground interaction. According to the rigid body kinematics (Chasles' theorem), the velocity vectors of each wheel center must be orthogonal to the joining segment of it with the chassis center O, but each of these velocity vectors cannot be generated directly, because of the non-steering characteristics and consequently, an axial sliding velocity component is produced at each wheel-ground contact, as sketched in the top view of Fig. 1. The other velocity vector component of each wheel center is well represented on the lateral view of Fig. 1, where the velocity diagrams of both wheels during their pure-rolling contact is shown by neglecting in this view, the abovementioned axial sliding motion, which is opposite between the front and rear axles. Of course, on this lateral view of Fig. 1, each wheel-ground contact point is supposed to be the instant center of rotation (IC) of the wheel, while the angular velocity vector $\boldsymbol{\omega}_{23}$ is given by the corresponding electric drive control. The wheel center velocity V is given by $V = \omega_{23}\, r$, where r is the wheel radius. The axial velocity diagrams are also shown.

3 Quarter-vehicle kinematic model

A three-dimensional quarter-vehicle kinematic model is proposed in the form of a spatial mechanism with a higher-pair at the wheel-ground contact, as shown in Fig. 2.

The main components are: the supporting plane (ground) 1; the rigid cylindrical wheel 2 of radius r; the chassis-link 3. In addition, this mechanism shows two revolute joints of the chassis-link 3 with the fixed vertical pin 1 and the rigid cylindrical wheel 2, respectively. Instead, the wheel-ground contact is sketched through a higher kinematic pair. The fixed reference frame $OXYZ$ is centered in O, which is also the origin of the chassis coordinate system of Fig. 1, where the same wheel is shown grey color. The wheel center O_{23} has coordinates ($p/2$, $-c/2$, 0) for a wheel thickness of d. This mechanism can work only because of the friction forces, which acts at the wheel-ground contact, otherwise the chassis-link 3 cannot be moved by the pure rotation of wheel 2.

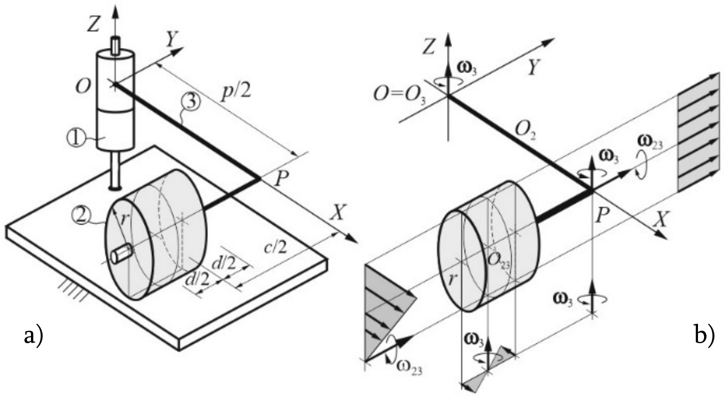

Fig. 2. Quarter-vehicle kinematic model: a) equivalent mechanism; b) velocity diagrams.

In fact, in the case understudy, the driving member is the wheel 2 and not the chassis-link 3, because there is not any driving torque acting on the vertical joint connecting 3 to 1 (ideal), but there is the action of the driving non-steering wheels, whose co-work to generate the vehicle rotation around the central vertical Z-axis.

Consequently, the whole kinematic behavior of the proposed equivalent spatial mechanism is shown in Fig. 2b, where the velocity vector field of the wheel 2 is decomposed into three velocity diagrams, which represent respectively, the pure-rolling motion of 2 on 1 in the vertical plane XZ, the pure-sliding motion of 2 on 1 in the vertical plane YZ and the spinning motion around the vertical axis passing through O_{23}. This decomposition of the velocity vector field can be better understood by considering the case of a vehicle driving rear axle with $p = 0$, which gives a spherical wheel motion. In particular, still referring to Fig. 2b, the chassis-link 3 rotates with the angular velocity ω_3 about the vertical Z-axis through the point $O = O_3$ and the wheel 2 rotates about its own axis with an angular velocity ω_{23}. It will be shown that they are kinematically related to each other. Thus, in order to generate the quarter-vehicle or the chassis-link 3 turning around its central vertical Z-axis, which coincides with the absolute I_3-axis, the front-right wheel 2 performs a compound motion, since it rotates about the revolute joint I_{23}-axis, but also around the axis of its central disk and passing through the O_{23} point while oriented according to the Z-axis. This corresponds to a spatial rigid motion along a proper instant screw axis (ISA), which satisfies the Aronhold–Kennedy theorem in three dimensions, as shown in Fig. 3. The front-right wheel — and similarly each of the remaining three wheels — rotates and translates respectively about and along their respective ISA. Consequently, the ISA I_2-axis of the wheel 2 has to be orthogonal to the common normal that is traced between the revolute joint I_{23}-axis and the chassis-link I_3-axis, also coinciding with the vehicle yaw axis. Figure 3 shows the results of this spatial kinematic analysis, along with the three axes I_2, I_3 and I_{23}, which satisfy the Aronhold-Kennedy theorem by sharing the X-axis as their common normal. The chassis-link 3 and the driving wheel 2 rotate about their corresponding I_3-axis and I_{23}-axis, with the angular velocity vectors $\boldsymbol{\omega}_3$ and $\boldsymbol{\omega}_{23}$, which can be expressed in matrix form, as follows

$$\boldsymbol{\omega}_3 = \begin{bmatrix} 0 & 0 & \omega_3 \end{bmatrix} \qquad \boldsymbol{\omega}_{23} = \begin{bmatrix} 0 & \omega_{23} & 0 \end{bmatrix} \tag{1}$$

The absolute angular velocity vector ω_2 of the driving wheel 2 with respect to the supporting plane 1 can be obtained by applying the Frisi theorem and thus, relating the angular velocity vectors $\boldsymbol{\omega}_2$, $\boldsymbol{\omega}_3$ and $\boldsymbol{\omega}_{23}$ as follows

$$\boldsymbol{\omega}_2 = \boldsymbol{\omega}_3 + \boldsymbol{\omega}_{23} = [0 \quad \omega_{23} \quad \omega_3] \tag{2}$$

which is solved by implementing the Eqs. (1). Thus, the magnitude of $\boldsymbol{\omega}_2$ takes the form

$$\omega_2 = \sqrt{\omega_3^2 + \omega_{23}^2} \tag{3}$$

Likewise, according to the Rivals theorem and considering the point P, at the chassis-link 3 corner, the corresponding punctual velocity vectors $\mathbf{v}_{P3}$ and $\mathbf{v}_{P2}$ of P as belonging to the chassis-link 3 (pure rotation) and to the driving wheel 2 (roto-translation), respectively, can be expressed as follows

$$\mathbf{v}_{P3} = \boldsymbol{\omega}_3 \times \mathbf{O}_3\mathbf{P} \tag{4}$$

$$\mathbf{v}_{P2} = \mathbf{v}_{2p} + \mathbf{v}_2 \tag{5}$$

where $\mathbf{O}_3\mathbf{P}$ is the position vector of point P with respect to the origin O_3, and in turn, $\mathbf{v}_2$ and $\mathbf{v}_{2p}$ correspond to the translation and rotation, along and through the I_2-axis, respectively, because of the screw absolute motion of the driving wheel 2. Thus, one has

$$\mathbf{O}_3\mathbf{P} = \begin{bmatrix} p/2 & 0 & 0 \end{bmatrix} \tag{6}$$

which can be substituted in Eq. (4), to give

$$\mathbf{v}_{P3} = \omega_3 \left(p/2 \right) \mathbf{j} \tag{7}$$

and in turn, the velocity vector $\mathbf{v}_{2p}$ takes the form

$$\mathbf{v}_{2p} = \boldsymbol{\omega}_2 \times \mathbf{O}_2\mathbf{P} = \omega_2 \left(p/2 - b_2 \right) \mathbf{j}, \quad \text{where} \quad \mathbf{O}_2\mathbf{P} = \begin{bmatrix} p/2 - b_2 & 0 & 0 \end{bmatrix} \tag{8}$$

Thus, the absolute chassis-link 3 motion is a pure rotation about the I_3-axis and the relative motion of the wheel 2 and the chassis-link 3 is also a pure rotation about the I_{23}-axis, while the wheel 2 performs a screw motion about the ISA I_2-axis.

Applying the Galilei theorem, it yields

$$\mathbf{v}_{P2} = \mathbf{v}_{P3} + \mathbf{v}_{P23} \tag{9}$$

and observing that $\mathbf{v}_{P23} = 0$, one has $\mathbf{v}_{P2} = \mathbf{v}_{P3}$. Referring to Fig. 3b, the screw motion of the wheel 2 about I_2-axis, is analyzed as follows

$$\mathbf{v}_{2p} = \mathbf{v}_{P3} \sin\theta_2 \tag{10}$$

and substituting the Eqs. (7) and (8) into the Eq. (10), one has

$$\omega_2 \left(p/2 - b_2 \right) \mathbf{j} = \omega_3 \left(p/2 \right) \mathbf{j} \sin\theta_2 \tag{11}$$

where the sine of θ_2 is given by

$$\sin\theta_2 = \omega_3 / \omega_2 \tag{12}$$

Moreover, substituting Eq. (12) into Eq. (11) and simplifying, the position b_2 of $O_2 = [b_2, 0, 0]$, along with the orientation θ_2, are given by

$$b_2 = \left(p/2 \right) \left[1 - \left(\omega_3 / \omega_2 \right)^2 \right] \qquad \theta_2 = \tan^{-1}\left(2r/c \right) \tag{13}$$

This formulation reveals that the wheel follows a screw-like trajectory, performing a double rotation — about its geometric I_{23}-axis and the vehicle vertical I_3-axis — while simultaneously translating along the screw I_2-axis. Therefore, in agreement with the Aronhold–Kennedy theorem in three dimensions, the driving wheel 2 performs a screw motion, while rotating around the revolute joint I_{23}-axis. In order to investigate the optimal theoretical shape of the wheel, one can consider the motion defined by the rotation of ISA I_2 around I_3, together with the rotation of I_2 around the I_{23}. The ISA I_3 can be expressed as a line in a three-dimensional space that passes through the point $O = [0, 0, 0]^T$ and directed along the unit vector $\hat{\mathbf{v}}_{I3} = [0, \ 0, \ 1]^T$, which coincides with fixed frame Z-axis. The parametric equation of axis I_3 is given by

$$\mathbf{r}_3(t) = \mathbf{O} + t\hat{\mathbf{v}}_{I3} \qquad t \in {}^{\sim} \tag{14}$$

The ISA I_{23}-axis, which is parallel to the Y-axis in the vehicle reference frame, can be defined as the straight line passing through the point O_{23} and directed toward the point $P = [p/2, 0, 0]^T$. The corresponding direction vector is

$$\mathbf{v}_{l23} = \mathbf{P} - \mathbf{O}_{23} = \begin{bmatrix} 0, & c/2, & 0 \end{bmatrix}^T \tag{15}$$

with the unit vector $\hat{\mathbf{v}}_{l23} = \mathbf{v}_{l23} / |\mathbf{v}_{l23}|$. The parametric form of the l_{23}-axis is given by

$$\mathbf{r}_{23}(t) = \mathbf{P}_3 + t\hat{\mathbf{v}}_{23} \qquad t \in \sim \tag{16}$$

Similarly, the ISA l_2, can be defined as the straight line passing through the point $O_2 = [b_2, 0, 0]^T$, which lies along the X-axis. The direction vector of this axis is

$$\mathbf{v}_{l2} = \begin{bmatrix} 0, & \cos\theta_2, & \sin\theta_2 \end{bmatrix}^T \tag{17}$$

with the corresponding unit vector is $\hat{\mathbf{v}}_{l2} = \mathbf{v}_{l2} / |\mathbf{v}_{l2}|$. Thus, the parametric form of l_2 is

$$\mathbf{r}_2(t) = \mathbf{O}_2 + t\hat{\mathbf{v}}_{l2} \qquad t \in \sim \tag{18}$$

The rotation matrix **R** to give the finite rotations between these axes takes the form

$$\mathbf{R} = \begin{bmatrix} u^2 + (1-u^2)\mathrm{c}\theta & uv(1-\mathrm{c}\theta) - w\mathrm{s}\theta & uw(1-\mathrm{c}\theta) + v\mathrm{s}\theta \\ uv(1-\mathrm{c}\theta) + w\mathrm{s}\theta & v^2 + (1-v^2)\mathrm{c}\theta & vw(1-\mathrm{c}\theta) - u\mathrm{s}\theta \\ uw(1-\mathrm{c}\theta) - v\mathrm{s}\theta & vw(1-\mathrm{c}\theta) + u\mathrm{s}\theta & w^2 + (1-w^2)\mathrm{c}\theta \end{bmatrix} \tag{19}$$

where cθ and sθ stands for cosθ and sinθ, respectively, and $\hat{\mathbf{k}} = \begin{bmatrix} u, & v, & w \end{bmatrix}^T$ is the unit vector defining the axis of rotation and $\theta \in [0, 2\pi]$. In particular, $\hat{\mathbf{k}} = \hat{\mathbf{v}}_{l3}$ when l_2 rotates around l_3, and $\hat{\mathbf{k}} = \hat{\mathbf{v}}_{l23}$ when it rotates around l_{23}. When ISA l_2 undergoes a rotation about either l_3 or l_{23}, its new orientation can be computed using Eq. (24), as follows

$$\mathbf{v}_{l2}^* = \mathbf{R}\mathbf{v}_{l2} \qquad\qquad \mathbf{O}_2^* = \mathbf{R}\mathbf{O}_2 \tag{20}$$

The equation of the rotated l_2-axis with respect to each reference axis is

$$\mathbf{r}_2^*(t) = \mathbf{O}_2^* + t\hat{\mathbf{v}}_{l2}^* \qquad t \in \sim \tag{21}$$

where $\hat{\mathbf{v}}_{l2}^*$ corresponds to the rotation of l_2 around either l_3 or l_{23}. Equation (21) is particularly useful for analyzing the shape of the wheel, the **resulting screw motions,** the **wheel-ground contact trajectories**, along with its rolling and sliding motions.

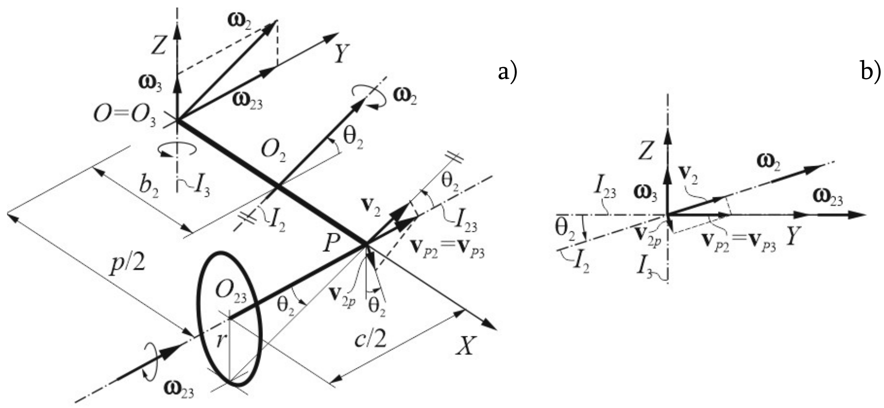

Fig. 3. Quarter-vehicle kinematic model: a) kinematic analysis; b) velocity vectors diagram.

4 Numerical Results

The proposed algorithm has been implemented in Matlab and validated numerically through representative examples of Fig. 4a and b, under the following conditions: the vehicle wheel base is $p = 2000$ mm; the track width is $c = 1400$ mm; the wheel radius is $r = 300$ mm; the angular velocity of the chassis around the vertical axis is $\omega_3 = 6.0$ rad/s; and the angular velocity of the wheel around its own axis is $\omega_{23} = 15.0$ rad/s. In particular, Fig. 4a shows a 3D visualization of the theoretical wheel shape (hyperboloid) that is derived by this spatial kinematic analysis. The velocity vectors are also shown at the wheel-ground contact point and the corresponding numerical results are:
$\omega_2 = 16.15$ rad/s; $b_2 = 862.0690$ mm; $\theta_2 = 23.1986°$; $v_{P2} = v_{P3} = 6\ 10^3$ mm/s; $v_2 = 5.5149\ 10^3$ mm/s and $v_{2p} = 2.3635\ 10^3$ mm/s. This approach has been extended to the other wheels and the algorithm result of Fig. 4b has been obtained, which shows the four wheels (hyperboloids), while the right wheels pair is rotating counter-clockwise in the positive direction of the Y-axis and the other two wheels on the left side, are rotating in the opposite sense. The front side of the vehicle is supposed to be along the positive X-axis as sketched in Fig. 1. This representation of the velocities highlights the complexity of the wheel-ground interaction, revealing that the contact dynamics cannot be completely captured by simple pure rolling assumptions.

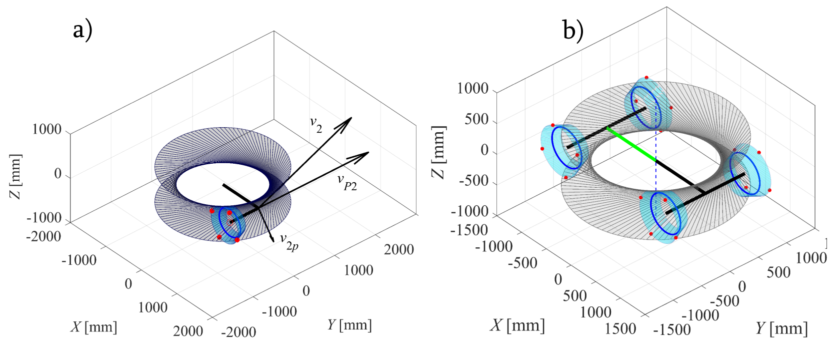

Fig. 4. Algorithm results: a) front-right wheel; b) four-wheels of the full vehicle

5 Conclusion

The kinematic analysis of non-steering four-wheel vehicles is presented by devoting particular attention to the turning task around the central vertical axis, which is obtained by rotating the right-side wheels pair in opposite sense, with respect to those of the left side. The proposed formulation has been implemented in Matlab by giving first significant graphical and numerical results, such as the axodes in the form of hyperboloids, which will be useful for further developments to design suitable wheels. Other results on the full vehicle are also shown to analyze the turning about the central vertical axis.

References

1. Figliolini, G., Rea, P.: Chapter 1: Mechanics and simulation of six-legged walking robots, Climbing & Walking Robots, Towards New Applications, I-Tech Education and Publishing, ISBN-978-3-902613-16-5, (2007).
2. Angeles, J.: Fundamentals of Robotic Mechanical Systems: theory, methods and algorithms, 4^{th} Ed., Mech. Eng. Series, vol. 124, Springer Int. Publ., Cham, Switzerland (2014).
3. Figliolini, G., Lanni, C., Angeles J.: Kinematic analysis of the planar motion of vehicles when traveling along tractrix curves. J. of Mech. and Rob., vol. 12, n. 5, pp.1–9 (2020).

4. Lanni, C., Figliolini, G., Tomassi L.: Roll center and centrodes of an eight-bar suspension system, In: Proc. of ASME 2023 IDETC & CIE in Eng. Conf., Boston, MA, USA, DETC2023-116901 (2023).
5. Lanni, C., Figliolini, G., Tomassi, L.: Kinematic and curvature analysis of the McPherson eight-bar suspension system. In: Proc. of ASME 2024 IDETC & CIE in Eng. Conf., Washington, DC, USA, Vol. 7: 48th Mech. and Rob. Conf. (MR), V007T07A004 (2024).
6. Tagliavini, L., Colucci, G., Botta, A., Cavallone, P., Baglieri, L., Quaglia, G.: Wheeled mobile robots: state of the art overview and kinematic comparison among three omnidirectional locomotion strategies. J. of Intelligent & Robotic Systems, vol. 106, n. 3, pp. 1–18 (2022).
7. Gracia, L., Tornero, J.: Kinematic modeling of wheeled mobile robots with slip. Advanced Robotics, vol. 21, pp. 1253–1279 (2007).